UC Santa Barbara

UC Santa Barbara Previously Published Works

Title

Ten-Year Landsat Classification of Deforestation and Forest Degradation in the Brazilian Amazon

Permalink

https://escholarship.org/uc/item/5h49j5bb

Journal

Remote Sensing, 5(11)

ISSN

2072-4292

Authors

Souza, Carlos M
Siqueira, João V
Sales, Marcio H
et al.

Publication Date

2013

DOI

10.3390/rs5115493

Peer reviewed

eScholarship.org Powered by the California Digital Library
University of California

Remote Sens. **2013**, *5*, 5493-5513; doi:10.3390/rs5115493

OPEN ACCESS

Remote Sensing

ISSN 2072-4292

www.mdpi.com/journal/remotesensing

Article

Ten-Year Landsat Classification of Deforestation and Forest Degradation in the Brazilian Amazon

Carlos M. Souza, Jr [1,*], João V. Siqueira [1], Marcio H. Sales [1], Antônio V. Fonseca [1], Júlia G. Ribeiro [1], Izaya Numata [2], Mark A. Cochrane [2], Christopher P. Barber [2], Dar A. Roberts [3] and Jos Barlow [4]

[1] Instituto do Homen e Meio Ambiente (Imazon), Rua Domingos Marreiros, 2020 Fátima, Belém, PA 66060-162, Brazil; E-Mails: joaovictor@imazon.org.br (J.V.S.); marcio@imazon.org.br (M.H.S.); antoniovictor@imazon.org.br (A.V.F.); juliagabriela@imazon.org.br (J.G.R.)

[2] Geospatial Sciences Center of Excellence, South Dakota State University, 1021 Medary Ave, Wecota Hall Box 506B, Brookings, SD 57007, USA; E-Mails: Izaya.numata@sdstate.edu (I.N.); mark.cochrane@sdstate.edu (M.A.C.); christopher.barber@sdstate.edu (C.P.B.)

[3] Department of Geography, University of California Santa Barbara, 3611A Ellison Hall, Santa Barbara, CA 93106, USA; E-Mail: dar@geog.ucsb.edu.

[4] Lancaster Environment Centre, Lancaster University, Lancaster LA1 4YQ, UK; E-Mail: jos.barlow@lancaster.ac.uk

* Author to whom correspondence should be addressed; E-Mail: souzajr@imazon.org.br; Tel.: +55-91-3182-4000; Fax: +55-91-3182-4027.

Received: 22 July 2013; in revised form: 18 October 2013 / Accepted: 18 October 2013 / Published: 28 October 2013

Abstract: Forest degradation in the Brazilian Amazon due to selective logging and forest fires may greatly increase the human footprint beyond outright deforestation. We demonstrate a method to quantify annual deforestation and degradation simultaneously across the entire region for the years 2000–2010 using high-resolution Landsat satellite imagery. Combining spectral mixture analysis, normalized difference fraction index, and knowledge-based decision tree classification, we mapped and assessed the accuracy to quantify forest (0.97), deforestation (0.85) and forest degradation (0.82) with an overall accuracy of 0.92. We show that 169,074 km^2 of Amazonian forest was converted to human-dominated land uses, such as agriculture, from 2000 to 2010. In that same time frame, an additional 50,815 km^2 of forest was directly altered by timber harvesting and/or fire, equivalent to 30% of the area converted by deforestation. While average annual outright deforestation declined by 46%

between the first and second halves of the study period, annual forest degradation increased by 20%. Existing operational monitoring systems (PRODES: *Monitoramento da Florestal Amazônica Brasileira por Satélite*) report deforestation area to within 2% of our results, but do not account for the extensive forest degradation occurring throughout the region due to selective logging and forest fire. Annual monitoring of forest degradation across tropical forests is critical for developing land management policies as well as the monitoring of carbon stocks/emissions and protected areas.

Keywords: deforestation; forest degradation; Amazon; decision tree

1. Background and Rationale

Brazil possesses a world treasure in its portion of the Amazon tropical rainforests, the largest contiguous forest area on the planet, encompassing around 4 million km^2 [1]. Roughly 20% of the original forest cover of this region has been converted to pasture, agricultural lands, and, to a lesser degree, urban areas, according to the Brazilian government forest monitoring program, named PRODES [2] (monitoramento da floresta amazônico por satélite; http://www.obt.inpe.br/prodes/index.php). Another major, but less understood source of change in this region is the degradation of standing forests. This occurs primarily through selective logging, forest fires and edge effects related to forest fragmentation [3,4]. Forest degradation may annually affect an area equal in magnitude to deforestation [5,6], and potentially be exacerbated by climate change and ocean temperature anomalies which may lead to more frequent droughts and longer dry seasons [7]. Most of this forest conversion has taken place in the past 40 years and Landsat observation can be used to detect, quantify and analyze deforestation and other land-use interactions and socio-environmental impacts [8].

Relationships and interactions among deforestation and forest degradation have been shown, but the extent to which they represent land cover dynamics across the basin and their variability in both space and time are still poorly quantified. Existing studies have either focused on local-to-regional scales with longer timespans, or larger areas with short temporal windows. For example, Landsat images from 1999 to 2004 have been used to assess the likelihood of selectively logged forests being cleared in four of the nine states of the Brazilian Amazon [9]; a combination of visual interpretation and semi-automated techniques were used to map selective logged forests in 1992, 1996 and 1999 [10]; and an assessment of the interactions among deforestation, forest fragmentation and biomass collapse of forest edges was conducted using a long time series of 23 years (1985–2008) covering six Landsat images path/row scenes located in Rondônia state [11], in the southern Brazilian Amazon. Subsequent work expanded the geographic coverage for this analysis to the entire Brazilian Amazon region [11], but shortened the temporal coverage to 10 years (2001–2010). Both examples evaluated one type of forest degradation process and its interaction with deforestation, and there are many other local and regional studies in the scientific literature (e.g., [10,12–16]) lacking complete analyses of the spatial and large temporal coverage of forest changes associated with deforestation and the major forest degradation drivers (*i.e.*, logging, fires and forest fragmentation). What is needed to better understand these interrelated forest disturbances is a high resolution, basin-wide product, similar to the PRODES

deforestation mapping effort, that is capable of monitoring deforestation, the resulting forest edges that isolate forest remnants, and forest degradation associated with selective logging and incursions of fire. Anthropogenic forest disturbance from logging and fires produces long lasting changes in forest structure and biomass [17–19], but these changes are hard to detect in satellite imagery [20] and are quickly obscured by the regenerating forest canopy [17,21]. Previous studies have shown that monitoring of forest degradation is possible using Landsat imagery but that annual imaging would be required to provide accurate tracking of its transitory signal [17,21].

2. Objectives

Our main objective here is to present in detail a methodology to process an extensive spatial and temporal series of Landsat imagery and classify forest cover changes associated with deforestation and forest degradation (logged and burned forests) (Figure 1). We applied these methods to a very large archive of Landsat images (1,465 scenes) covering the Brazilian Amazon and encompassing 11 years (2000–2010). Our second objective was to assess the accuracy of our classified products using a higher spatial resolution SPOT imagery dataset, and field-collected degradation data from 151 forest transects. We also compared our annual estimates of deforestation rates with available deforestation data from PRODES [2] for the Brazilian Amazon region and discuss the potential to apply our approach to other tropical forest regions.

Figure 1. Forest degradation processes and interactions commonly found in the Brazilian Amazon. Pristine forests can be subject to selective logging, creating favorable conditions for burning when fires from adjacent agriculture fields unintentionally escape. Logging and fires can be recurrent, creating highly degraded forests. Eventually, degraded forests can be converted by deforestation, increasing forest edges and landscape fragmentation [8]. If degraded forests are not cleared, vegetation regeneration processes can prevail given the high resiliency of forests (Source: [3]).

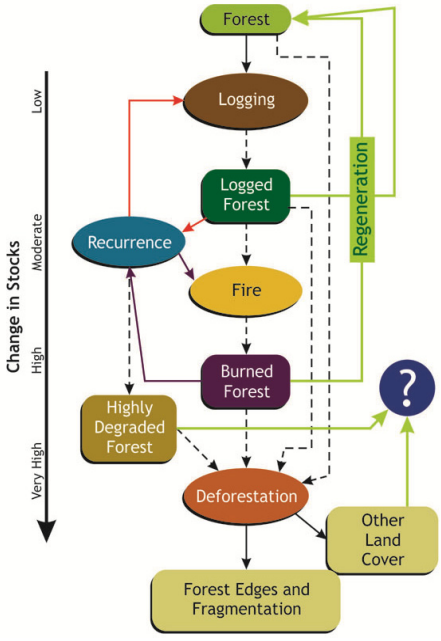

3. Methods and Study Region

We used 1,465 Landsat Thematic Mapper (TM)/Enhanced Thematic Mapper (ETM+) images acquired during the 2000–2010 time period, covering most of the Brazilian Amazon Biome, to detect and map deforestation and forest degradation. The great majority of the images had a maximum cloud cover of 20%, but imagery with cloud cover up to 30% was occasionally used. Due to the lack of cloud-free Landsat images, the annual area mapped ranged from 106 to 157 images, out of a possible coverage of 192 for the entire study region (Figure 2), encompassing roughly 4 million km^2. Most of the missing scenes were from the wetter and less populated portions of the study area. The southern and eastern regions of the Amazon, where the vast majority of deforestation and forest degradation take place, were well covered in all years.

Figure 2. Landsat TM/ETM+ images used in mapping deforestation and forest degradation. A total of 1,465 images were acquired, predominantly (90%) from the image server of the National Institute for Space Research (INPE).

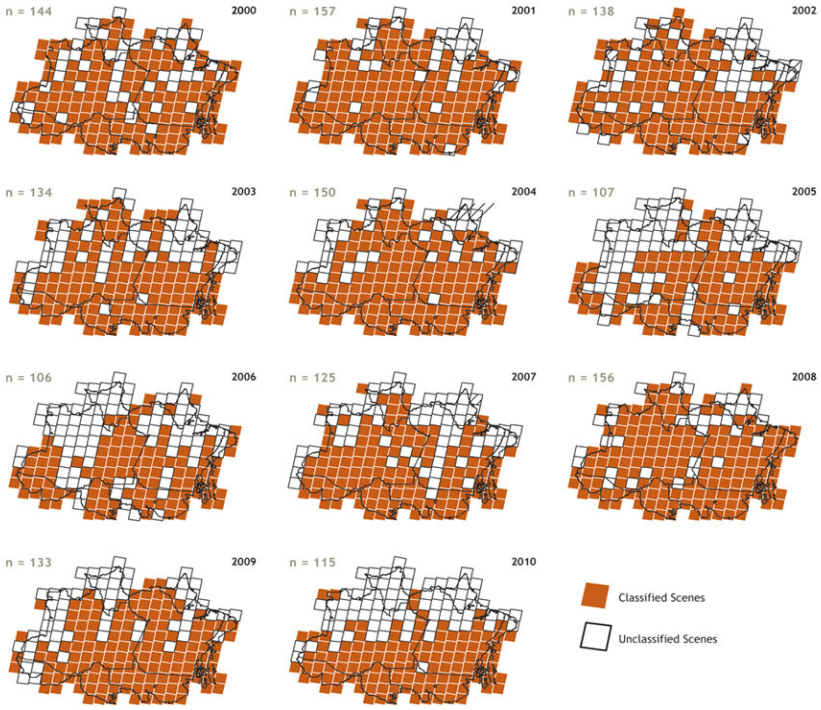

Data from the satellite images were radiometrically normalized, converted to surface reflectance, and quantitatively analyzed to enable establishment of automatic, generic and consistent classification rules. We applied computing rules to detect possible classification inconsistencies over time and adjusted classification rules to correct for these problems. Finally, the maps generated with automatic classification were inspected and manually edited by analysts in order to correct residual misclassification errors. Map results were then tabulated and used to estimate annual deforestation and forest degradation rates. Annual periods used the reference date of 1 August (e.g., annual deforestation for the year 2001 is obtained for the period of 1 August 2000 through 31 July 2001; and so on for the following years) to match the protocol used officially by the Brazilian government (INPE-PRODES [2]).

Figure 3 illustrates the flow of the image processing procedures. Detailed descriptions of the individual image processing procedures are presented in sequence below.

Figure 3. Flow of the image processing procedures as implemented with an ImgTools conceptual framework (**a**) including: (1) pre-processing, (2) spectral endmember library development, (3) Spectral Mixture Analysis (SMA); (4) Image Classification, and (5) Post-Classification processing and assessment. Most of the routines of this framework were implemented in ImgTools software [22] (**b**).

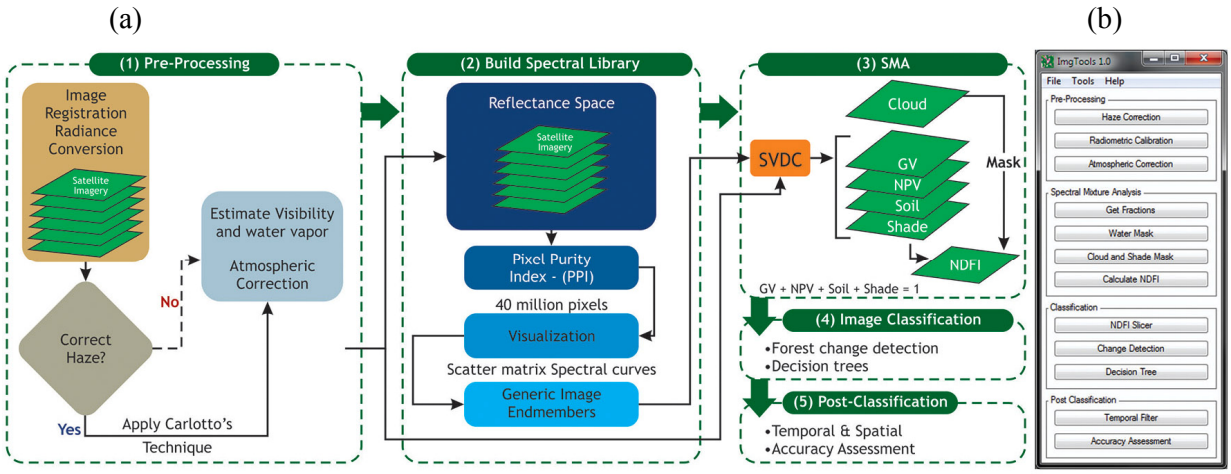

3.1 Image Processing

3.1.1. Pre-Processing

Our image classification approach requires pixel co-registration accuracies of <1 pixel to perform annual and multi-year forest change detection and image classification [3,21,22]. Image registration was performed using Delauney triangulation and nearest neighborhood resampling, available in ENVI 4.7 software, with enough image control points (usually 10–20) to provide low root mean squared (RMS) errors (*i.e.*, <1 pixel) that minimize misregistration errors in land cover changes detected over time [23].

Correction of spatially variable atmospheric contamination noise due to haze and smoke [24] was implemented in ImgTools [22]. The Carlotto technique assumes that smoke and haze primarily impact the visible bands, leaving the near-infrared (NIR) and short-wave infrared (SWIR) bands unaffected. Statistics are calculated for the entire image, in which average values for visible bands (e.g., bands 1, 2 and 3 for Landsat TM/ETM+) are calculated for each unique combination of NIR and SWIR bands (e.g., bands 4, 5 and 7 for Landsat TM/ETM+). After calculating these statistics, the original values for the visible bands for a specific combination of the NIR and SWIR bands are replaced with the scene averages for that combination. This technique homogenizes contamination throughout a scene; thus, clear sky portions of the image gain a slight amount of contamination, while contamination is significantly reduced in areas under smoke or haze, providing atmospheric correction that improves overall image quality.

Following the pre-processing steps, we used ImgTools software [22] to perform radiometric correction of the Landsat satellite data using the gains and offset provided in the image metafile. Radiance data was converted to reflectance using other software (Atmospheric Correction Now, ACORN 4.0, ImSpec LLC, Boulder, CO, USA; or FLAASH ENVI module). More detail about these steps can be found elsewhere [21].

3.2. Spectral Mixture Analysis (SMA)

SMA decomposes the spectral mixture—commonly found in the pixel reflectance values of remotely sensed data—into fractions of purer materials, known as endmembers (EM) [25]. ImgTools [22] was used to perform all SMA procedures described below, including the Normalized Differencing Fraction Index (NDFI) calculation [21]. The SMA model assumes that image spectra are formed by linear combinations of *n* pure spectra [26], such that:

$$R_n = \sum_{i=1}^{n} F_i \, R_{i,b} + \varepsilon_b \tag{1}$$

for

$$\sum_{i=1}^{n} F_i = 1 \tag{2}$$

where R_b is the reflectance in band b, $R_{i,b}$ is the reflectance for endmember *i*, in band b, F_i is the fraction of endmember *i*, and ε_b is the residual error for each band. The SMA model error is estimated for each image pixel by computing the Root Mean Square (RMS) error, given by:

$$RMS = [n^{-1} \sum_{b=1}^{n} \varepsilon_b]^{1/2} \tag{3}$$

SMA has been applied extensively in studies of the Amazon region used to generate fractions images used as input variables in subsequent image classification techniques [26,27] or to estimate biophysical properties of vegetation and soils [17,28–30]. The SMA model results were evaluated following a standard protocol to assess SMA results [26]. First, the RMS images were inspected and models with RMS values greater than 5% were discarded from the fraction change analysis. Next, fraction images were evaluated and interpreted in terms of field context and spatial distribution. Finally, histograms of the fraction images were inspected to quantify the percentage of pixels lying outside the range of 0%–100% and to evaluate fraction value consistency over time (*i.e.*, that intact forest values were similar over time). Only models that showed mean fraction value consistency over time and had at least 98% of the values within 0%–100% were utilized. Models that did not pass one of these tests resulted in the image processing being redone with new parameter models (*i.e.*, visibility, atmosphere type, *etc*.) for the atmospheric correction and repetition of each of the subsequent steps.

3.2.1. Building the Endmember Spectral Library

Standard global EM from the Landsat n-dimensional spectral space has been proposed [31]. We used this approach to standardize EM to determine generic image of green vegetation (GV),

non-photosynthetic vegetation (NPV) and soil to generate standard fraction images of these EM over the Brazilian Amazon [21].

Identification of the nature and number of pure spectra (*i.e.*, EM) in the image scene is imperative for a successful application of SMA models. Four EM are expected in forested environments: GV, NPV, Soil and Shade [21,32]. We applied a Cloud endmember to facilitate cloud masking. Image EM representing GV, NPV, Soil and Cloud were extracted from reference reflectance images selected across the region. The Shade endmember was assigned zero percent reflectance at all wavelengths (photometric shade). The pixel-purity-index (PPI), available in ENVI 4.0 [33], was used to identify image endmember candidates. Five image subsets (500 × 500 pixels), representing the variety of land cover types found in 40 Landsat images, were used as inputs for the PPI algorithm. The PPI results were used to identify pixel locations in the original image and extract the associated spectral curves. Final image EM were selected based on pixel location in the Landsat reflectance spectra with the aid of an n-dimensional visualization tool available in ENVI. The pixels located at the extremes of the spectral data were selected as candidate EM. Final EM were selected based on the spectral shape and image context (e.g., soil spectra are mostly associated with unpaved roads and NPV with pasture having senesced vegetation). ImgTools provide a set of generic EM for Landsat sensors obtained using the procedures described above.

3.2.2. Normalized Difference Fraction Index (NDFI)

To enhance the degradation signal caused by selective logging and forest burning, the Normalized Difference Fraction Index (NDFI) [3,21] was computed using the fraction images obtained with SMA:

$$\mathrm{NDFI} = \frac{\mathrm{GV}_{\mathrm{Shade}} - (\mathrm{NPV} + \mathrm{Soil})}{\mathrm{GV}_{\mathrm{Shade}} + \mathrm{NPV} + \mathrm{Soil}} \tag{4}$$

where GVs_{hade} is the shade-normalized GV fraction given by,

$$\mathrm{GV}_{\mathrm{Shade}} = \frac{\mathrm{GV}}{100 - \mathrm{Shade}} \tag{5}$$

NDFI values range from −1 to 1. Theoretically, NDFI values in intact forest are expected to be high (*i.e.*, about 1) due to the combination of high GVs_{hade} (*i.e.*, high GV and canopy shade) and low NPV and soil values. As the forest becomes degraded, the NPV and soil fractions increase due to the diminished canopy cover, lowering NDFI values relative to intact forests. The synthetic NDFI band combines all reflectance information shown to be relevant for identifying and mapping degraded forests in the Amazon region [3,21].

3.3. Image Classification

Image classification techniques were implemented in ImgTools [22] to speed up the extraction of information from satellite imagery through a Generic Classification Algorithm (GCA). The overall principle of GCA relies on: (i) normalized and noise reduced data sets; (ii) specific objectives regarding information extraction; (iii) combination of spectral, spatial and temporal pixel information to detect and map specific targets; and (iv) minimal analyst interference to check for misclassification

errors, most likely to happen when images are extensively covered by clouds. We used a knowledge-based decision tree classification (DTC) that implements hierarchical classification rules obtained through a recursive partition process of classification training samples or knowledge-based (*i.e.*, empirical) classification rules. A default set of empirical knowledge-based rules is provided in ImgTools, obtained from extensive tests over the study region [3,22].

We used fraction images obtained from SMA as data input variables for classification using the GCA tree rules (Figure 4). The variables selected for the GCA are indicated in the internal node and the final classes as terminal nodes. The first step, at the tree root level of this binary hierarchical classification process, was the masking out of cloudy areas. To do this, we used the input variable cloud fraction (V_{cloud}) obtained from SMA. When $V_{cloud} \geq 10\%$, image pixels were classified as Cloud which is a terminal node. Pixels that did not satisfy this condition were classified as No-Cloud and further classification rules were applied. V_{GVs} provide the abundance of green vegetation with pixels and played an important role in separating forest and non-forest areas. Pixels with $V_{GVs} \geq 85\%$ are associated with croplands and young (*i.e.*, <10 years old) second growth forests and, therefore, were classified as Deforestation (*i.e.*, previously deforested areas). Forests with high $V_{NDFI} \geq 0.75$ were classified as Forest (NDFI variable was rescaled to 0–200, meaning that $V_{NDFI} \geq 175$ in Figure 4 translates to $V_{NDFI} \geq 0.75$). Then, forested pixels that did not satisfy "$V_{NDFI} \geq 0.75$" (*i.e.*, low NDFI values) were classified as [Forest] Degradation. This forest degradation class represents canopy damage areas created by selective logging and/or forest fires, *i.e.*, only canopy damage >25% can be detected. The Water class was obtained with low V_{GVs} and low $V_{NPV+Soil}$ abundance (Figure 4). All the variables and the decision tree rules selected translate into expected biophysical responses of the environments we aimed to map.

Figure 4. Empirical decision tree used for classifying deforestation and forest degradation. NDFI variable was rescaled to 0–200, meaning that $V_{NDFI} \geq 175$ translates to $V_{NDFI} \geq 0.75$.

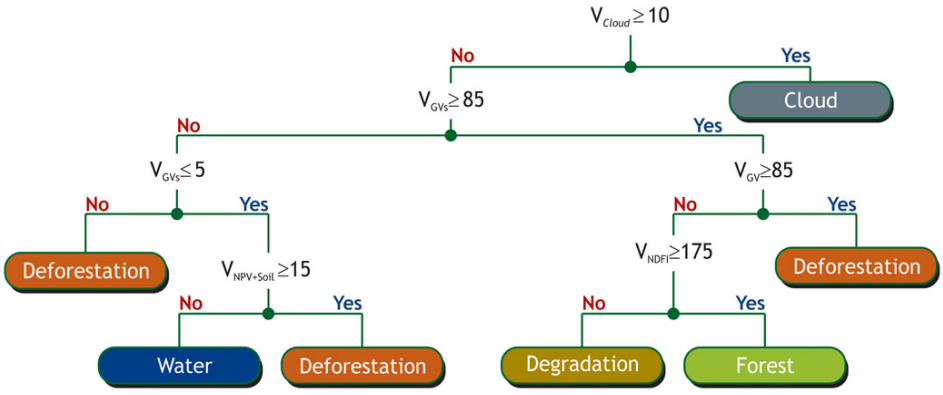

3.4. Post-Classification

Post-classification processing included application of spatial and temporal image filters. The spatial filters implemented in ImgTools reduced classification noise based on area label size. For that, we used the label region function implemented in the Interactive Data Language (IDL version 5.0) to identify regions in the classified images formed by each individual class. The label region function assigns the area size of the regions for each specific thematic class. Then, we set minimum and maximum area

values to identify spurious or individual pixels in the classified images and substitute them by a majority class neighborhood values. For example, isolated classified regions with 1–3 pixels were reclassified using this procedure which smoothed small features such as individual treefalls or forest edge pixels that would otherwise inflate forest degradation amounts. A temporal filter was used to correct for disallowed classification transitions over time (e.g., a forest to non-forest to forest transition occasionally seen along forest edges) and to remove cloud pixels when possible [16]. For example, if a given class (forest or non-forest) existed both before and after an area was classified as being cloud, then no land cover change was believed to have occurred during the short interval (*i.e.*, <3 years). Therefore, clouds were removed and reassigned to the appropriate class.

3.5. Accuracy Assessment

For accuracy assessment, we used the protocol defined by [34]. This protocol applies a series of procedures for statistical selection of reference samples, evaluation and labeling (or classification) rules of reference data, and unbiased corrections of the reference data (e.g., geolocation, mixed pixels, edges, and reference data classification errors), to eliminate errors in the processing. Very high spatial resolution SPOT 2.5 m pixel imagery was used to generate geolocated points to assess the accuracy of the classified images. These images were acquired from 2007 to 2010 and these dates were matched with the classified images dates for comparing referenced data and classified results (Figure 5).

Figure 5. Location of SPOT very high-resolution imagery and forest transects used for accuracy assessment of forest, deforestation and forest degradation classes.

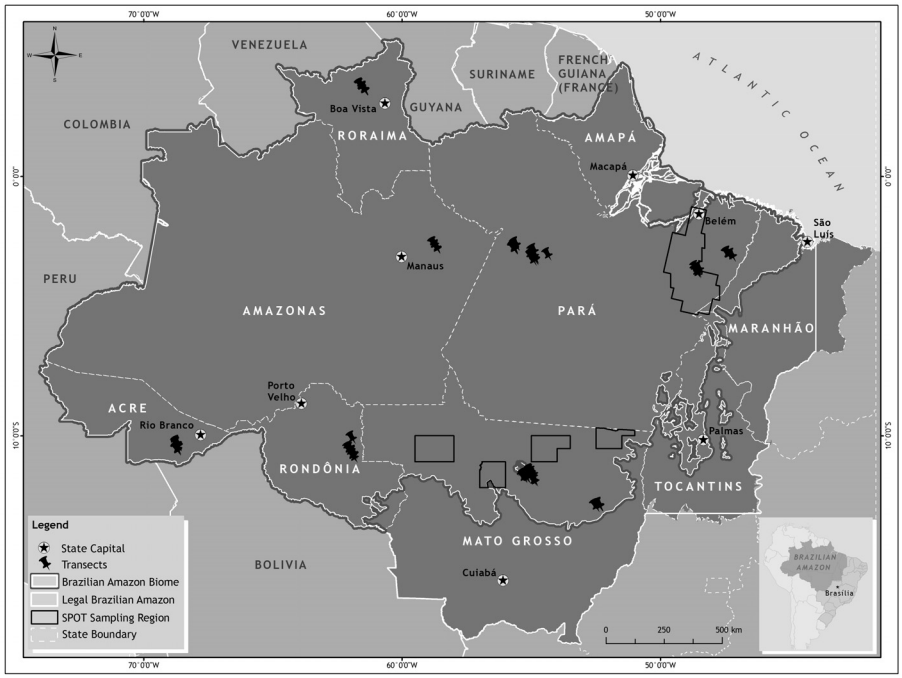

A total of 1,980 points were interpreted by five independent image analysts covering about 10% of the area of the states of Pará (n = 500) and Mato Grosso (n = 1,480), where most degraded forests are expected [6]. Because the random selection of points on the SPOT imagery used for the accuracy

assessment did not include enough points in degraded forests (40 points only), we added independent forest transects (n = 151) in this analysis. Ground collected transects covering 10 × 500 m (0.5 ha), were used from two sources: [35] (n = 49) and Barlow (unpublished data; 48 transects and 102 data points along them). The combined reference points were used to obtain an error matrix and statistical measures of accuracy. Of the total points (2,131 obtained from combined SPOT 2.5 imagery and forest transects), only 1,605 (1,454 SPOT plus 151 transects) points were used in the final accuracy assessment. Several points occurred in water bodies (n = 231) and were not included in the analysis because the map accuracy for this class was very high and this would inflate the overall map accuracy. The other points were removed due to the lack of matching dates between the Landsat and SPOT scenes, geolocation errors, or mixed classes (e.g., 50% of forest and 50% of deforestation) or cloud cover either in the Landsat or SPOT scene. Using low quality reference data can result in drastic underestimates of the accuracy assessments of results and these types of corrections for reference data have been proposed to avoid this problem. We also evaluated the impact on the accuracy assessment results when applying the corrections on the reference data [34].

Classification labeling rules were applied to the SPOT 2.5 imagery to assign thematic classes to sample units, defined as the Landsat pixel size. We used slightly modified class definitions proposed in a previous study [34] to map the reference data, as follows: (i) Primary forest: trees >20 m in height, continuous canopy; (ii) Second-growth forest: shrubs >2 m in height, trees <2 m height, perennial crops; (iii) Pasture: shrubs <2 m in height, herbaceous vegetation, sparse canopy, annual crops; (iv) Urban/bare Soil: human-built structures, roads, bare soil; (v) Water: open water surfaces. In our final classification scheme, we merged the Pasture and Urban/Bare Soil classes with the Deforestation class, and the Forest Degradation class was classified as discontinuous Primary Forest with perforations with exposed soils and canopy damage >25%. The majority class rule was applied to assign a final class to mixed pixels. Pixels with equal class proportions were assigned as mixed pixels and were not used in the accuracy assessment process. The forest transects were labeled based on ground assessment as two classes: Forest and Forest Degradation. As a result, we compared two thematic maps to assess the map accuracy: one obtained with Landsat imagery and another with the reference labeling process described above. Figure 6 illustrates how labeling of reference data (SPOT 2.5 imagery) was conducted and the comparison with the map results from Landsat.

3.6. Estimating the Annual Rate of Forest Changes

Annual rates of the area of forest affected by deforestation or forest degradation processes, in any given year, are expressed in absolute terms of square kilometers per year. Brazil uses August 1 as the reference date for estimating each year's annual deforestation rates in its PRODES products [2]. To provide comparable estimates, we also adopted the period of 1 August to 31 July as the reference period for each year. Because of frequent regional cloudiness [36], haze and the 16-day repeat cycle of Landsat satellite imagery, monitoring efforts in the Brazilian Amazon, including this study, cannot always acquire imagery on or near the reference period date used for estimating the annual rate. It is thus necessary to project measurements made with satellite data for the remaining period of reference by using mathematical methods.

Figure 6. Example of annual deforestation and forest degradation classification results obtained with a temporal series of Landsat images using the methodology presented in this study (**a**). For base year (2000), we mapped all of the areas already deforested and without forest cover (e.g., rivers, savannas) to generate a reference forest map (including areas already degraded). Early state secondary forests were removed from the forest baseline map by applying a mask of deforested areas identified by PRODES up to 2000 [2]. The annual maps are used to generate maps of age of deforestation (**b**) and forest degradation, and forest degradation frequency maps. All this information was produced for the entire forest biome of the Brazilian Amazon (**c**).

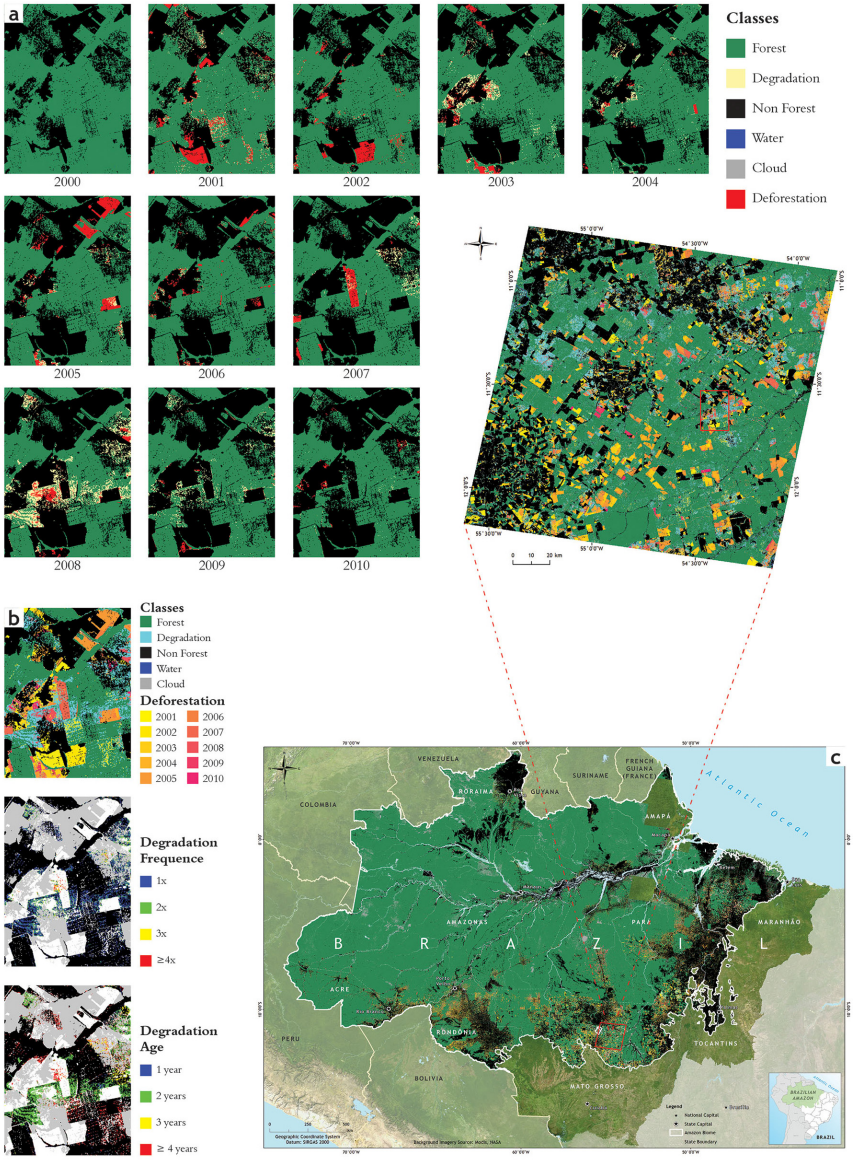

We adopted the method proposed by the Food Administration Organization [37] to estimate annual deforestation rates in this study. We calculated the annual percentage rate of forest cover lost using the method suggested by [38]. The area of forest lost to deforestation is assumed to decrease over time at an exponential rate, given by:

$$r_{(t-1,t)} = \left(\frac{1}{t2 - t1}\right) \times ln\left(\frac{A_{t2}}{A_{t1}}\right) \quad (6)$$

where A_{t1} and A_{t2} are the forest areas mapped in times t_1 and t_2, expressed in years, beginning with an initial year (t_0 = 2,000). The result ($r_{(t-1,t)}$) represents the percentage rate of forest loss normalized for the period between t_2−t_1 (in years). With the value of r it is possible to calculate the annual deforestation rate (D_t in km^2/year) for the given reference period as:

$$D_t = A_{t-1} \times (1 - e^{r_{t-1,t}}) \quad (7)$$

For example, for t = 01/08/2001 and $t - 1$ = 01/08/2000 the annual deforestation rate in Equation (7) is obtained by:

$$D_{2001} = A_{2000} \times (1 - e^{r_{2000,2001}}) \quad (8)$$

where the rate $r_{2000,2001}$ is calculated using Equation 6, with acquisition dates and resulting area data from images obtained during 2000 and 2001. In the example above, A_{2000} is the initial forest area projected or observed on 1 August 2000. For subsequent years, D_t is the annual deforestation rate, normalized for the reference period between the years $t - 1$ and $t_{(2001,\ldots,2010)}$, and A_{t-1} is given by A_{t-2}-D_{t-1}, for t (2001,...,2010).

To calculate the annual rates for individual Amazonian states, we applied a mask of the state boundaries on a per scene basis, in order to apply this method only in the portions of a given state covered by the scene. For cases with gaps of one or more years between Landsat images, we assumed a steady rate of deforestation between observations, using the same estimate of r for all intervening years between the two acquired images. Deforestation observed in imagery after temporal gaps caused by cloud cover were distributed equally across the reference periods in which clouds occurred. For example, if a newly deforested area of X km^2 is observed in 2003, but the area was obscured by clouds during 2001 and 2002, we assume that X/3 km^2 of clearing happened in each of the three years between observations.

The same methodology described above was applied for estimating the annual rate of forest degradation, discounting the annualized deforestation for each period of reference to obtain the area of remaining forest in the respective year.

4. Results

Our image processing methodology simultaneously mapped deforestation and forest degradation caused by logging activity and forest burning using Landsat satellite images. Methods that individually detect and estimate deforestation and forest degradation are prone to substantial uncertainty and confusion among classes due to differing classification thresholds. For example, severe forest degradation can be confused with intentional forest clearing in regional deforestation estimates [39] if forest damaging events are not accounted for in the classification process. Deforestation is an ongoing process of converting forested land to other land uses, such as pastures, agricultural fields, mining, or regional urbanization [3]. In deforestation there is near-complete removal of the original forest cover, while forest degradation events only partially and temporarily remove forest canopy cover. The forest change detection methodology we present in this study simultaneously maps deforestation and forest

degradation, reducing possible zones of "confusion" between these classes of land cover change (Figure 6a). Additionally, it provides information on deforestation and forest degradation ages, and of forest degradation frequency (Figure 6b), and was applied to the entire Amazon biome (Figure 6c). We present these results below and assess the accuracy of the proposed method to account for simultaneous mapping of deforestation and forest degradation.

4.1. Accuracy Assessment

We used a random selection of geolocated points from within the SPOT scenes but this process only produced a limited number of points for the forest degradation class (n = 26), insufficient for assessing classification accuracy. For this reason, we used independent forest transects to complement the imagery-based reference data and enable the adequate accuracy analysis. The overall accuracy for mapping forest, forest degradation and deforestation was 0.92 using either the SPOT 2.5 imagery as reference data (Table 1a) or the combination of this data with forest transects (Table 1b). However, using SPOT imagery alone as reference data indicated a very low user's accuracy for the forest degradation class due to the low sample size (50%). Combining forest transect data with SPOT 2.5 created a more robust reference dataset to assess this class, leading to a more realistic user's accuracy for the forest degradation class of 0.76 (Table 1b) within the range of accuracy reported in previous works [6,13]. The impact on the accuracy assessment results when applying the corrections to reference data was also quantified. The overall accuracy went from 0.79 with no correction to 0.92 with all types of corrections applied (Table 1c). Even though we used a large random data set of reference data, combining SPOT 2.5 imagery and independent field transects, a more robust probability based sample for validation, implemented over larger areas and different image dates, would provide improved validation results.

4.2. Annual Rates of Deforestation and Degradation

The annual deforestation and forest degradation estimates for the 10-year study period are presented for each Amazonian state and for the region as a whole in Table 2. Rates were annualized on scene by scene bases (see methods) to normalize the variable observation dates to each year's annual reference period in accord with standard practices to provide comparable interannual results (Figure 7a).

For the interval between 2000 and 2010, we estimate 169,074 km^2 of Amazonian forest was deforested (Table 2a). An additional 50,815 $km^2$of forest was altered by timber harvesting and/or burning, equivalent to 30% of the area converted by deforestation (Table 2b). There was a substantial range of annual deforestation rates, with the peak deforestation rate occurring in 2004 (24,446 km^2/yr), and the lowest rate in 2010 (5,496 km^2/yr). Annual rates of deforestation have trended noticeably lower since 2005 (Table 2a). Annual forest degradation rates did not vary as much or have any noticeable trend, with a peak of 8,396 km^2/yr in 2008 and a minimum annual rate of 3,731 km^2/yr in 2010 (Table 2b). Degradation rates corresponded to a low percentage of 17% of deforestation rates in 2003 and a high of 68% in both 2008 and 2010.

Table 1. Accuracy assessment of the classification results using high spatial resolution SPOT data only (**a**), SPOT and forest transects (**b**) and the impact of applying corrections to the SPOT reference data on the accuracy results (**c**).

(**a**)

Reference Data (SPOT)

Land Cover Class	Forest	Degradation	Deforestation	Row Total	User's Accuracy	User's Standard Deviation
Forest	884	2	22	908	0.97	0.006
Degradation	6	20	14	40	0.50	0.080
Deforestation	60	14	432	506	0.85	0.016
Column Total	950	36	468	1,454	-	-
Producer's Accuracy	0.93	0.56	0.92	-	-	-
Producer's Standard Deviation	0.008	0.084	0.013	-	-	-
Overall Accuracy = 0.92 (0.007)						

(**b**)

Reference Data (SPOT + Transects)

Land Cover Class	Forest	Degradation	Deforestation	Row Total	User's Accuracy	User's Standard Deviation
Forest	942	11	22	975	0.97	0.005
Degradation	8	102	14	124	0.82	0.035
Deforestation	60	14	432	506	0.85	0.016
Column Total	1,010	127	468	1,605	-	-
Producer's Accuracy	0.93	0.80	0.92	-	-	-
Producer's Standard Deviation	0.008	0.036	0.013	-	-	-
Overall Accuracy = 0.92 (0.007)						

(**c**)

Influence of Reference Data (SPOT) "Corrections" on Map Accuracy

Version	Correction to Reference Data Set	Number of Samples	% Overall Agreement
1	None	1,725	0.79
2	Geocorrection	1,644	0.83
3	Geocorrection; Map edge	1,600	0.86
4	Geocorrection; Mixed pixel; Map edge	1,594	0.86
5	Geocorrection; Change pixel	1,502	0.89
6	Geocorrection; Change pixel; Mixed pixel	1,498	0.89
7	Geocorrection; Change pixel; Mixed pixel; Map edge	1,454	0.92

Excluded Samples

Reason for Exclusion	Number of Samples
No Data	3
Geocorrection	81
Change pixel	142
Mixed pixel	4
Map edge	44
Cloud	21
Water	231

The 10-year series of deforestation rates show high and fairly stable rates of deforestation for the 2001–2005 period (average 21,893 km^2/yr) with substantially reduced (46% lower) and declining deforestation rates from 2006 to 2010 (average 11,922 km^2/yr). Forest degradation rates did not show the same pattern, with an average annual rate of 4,627 km^2/yr for 2001–2005 and a larger 5,536 km^2/yr for 2006–2010, a 20% increase (Figure 7a).

The states contributing the greatest amounts of deforestation over the total period analyzed were Pará (35%) and Mato Grosso (31%), followed by Rondônia (16%) and Amazonas (10%) (Figure 7b). The state of Mato Grosso led in terms of forest degradation, contributing 48% of the total for the decade studied. Pará was second ranked in forest degradation with 32%, while Rondônia (7%) and Acre (5%) contributed much less (Figure 7c).

Table 2. Estimates of annual rates of deforestation (**a**) and forest degradation (**b**) obtained with Landsat images for the period of 2000–2010, using the image classification methodology presented in this study.

(a) Annual rates of deforestation (km^2/yr)

States	2001	2002	2003	2004	2005	2006	2007	2008	2009	2010	Total
Acre	487	948	640	819	851	521	545	256	495	203	**5,765**
Amapá*	-	-	-	-	-	-	-	-	-	-	**-**
Amazonas	1,482	2,475	1,682	2,010	2,031	1,673	1,306	1,115	1,535	917	**16,227**
Maranhão	676	371	402	329	524	389	433	588	918	236	**4,866**
Mato Grosso	5,905	7,527	8,735	10,463	6,959	4,142	3,026	3,055	1,215	1,221	**52,249**
Pará	4,516	8,139	6,194	6,664	7,625	6,184	5,888	5,284	6,693	2,480	**59,668**
Rondônia	3,525	2,983	3,752	3,665	3,973	2,820	2,316	1,835	1,025	346	**26,241**
Roraima	507	749	752	431	170	176	194	189	40	0	**3,209**
Tocantins	104	150	71	65	109	80	43	81	54	93	**849**
Amazon	**17,203**	**23,342**	**22,229**	**24,446**	**22,242**	**15,986**	**13,751**	**12,403**	**11,976**	**5,496**	**169,074**

(b) Annual rates of forest degradation (km^2/yr)

States	2001	2002	2003	2004	2005	2006	2007	2008	2009	2010	Total
Acre	157	441	185	65	48	731	549	282	133	71	**2,663**
Amapá *	-	-	-	-	-	-	-	-	-	-	**-**
Amazonas	94	118	146	232	224	206	208	236	151	41	**1,656**
Maranhão	58	171	25	20	154	382	51	677	145	122	**1,806**
Mato Grosso	3,033	2,198	2,208	2,459	2,359	1,878	1,516	4,956	2,331	1,625	**24,562**
Pará	1,007	1,382	1,114	1,707	1,509	2,659	1,566	1,829	1,654	1,785	**16,212**
Rondônia	293	408	179	541	380	601	453	378	269	70	**3,573**
Roraima	58	10	8	15	8	7	7	6	0	0	**118**
Tocantins	27	24	23	29	19	20	17	33	19	16	**226**
Amazon	**4,726**	**4,754**	**3,887**	**5,068**	**4,700**	**6,483**	**4,367**	**8,396**	**4,703**	**3,731**	**50,815**

***** It was not possible to estimate the annual rate for Amapá state due to the low number of observations with Landsat images during the period analyzed (only 27 out of 143 possible scenes with low cloud cover).

Figure 7. Historical changes of deforestation and forest degradation in the Brazilian Amazon for the period of 2000–2010 as obtained with the annualization method described in the methods (**a**). In (**b**) and (**c**) we present the Amazon state contributions of deforestation and forest degradation, respectively.

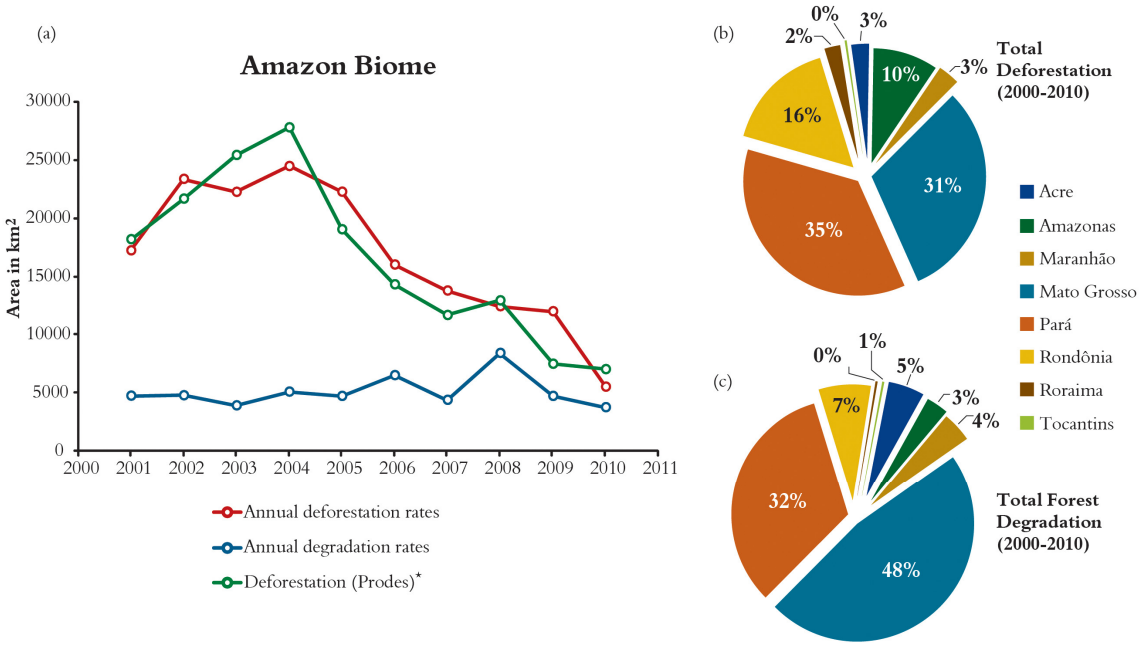

5. Discussion

Due to their scientific, conservation, and climate policy importance, forest degradation processes have been extensively studied in the Brazilian Amazon at local and regional scales through field studies [40], remote sensing observations [4,6,27], and models of ecological and land cover change [5,12,41]. To date, however, there have been no basin-wide estimates of the amount of forest affected by these processes. In a review of the remote sensing techniques applied for such work in the Brazilian Amazon, our research group has proposed [3] a framework for integrating deforestation and forest degradation monitoring activities to assess annual rates of both that would be capable of accounting for forest degradation age (time since disturbance) and recurrence rates (multiple logging and/or fire events) that could be used to better estimate remaining forest carbon stocks, and forest fragmentation. The methods and results presented here demonstrate the potential of this monitoring framework to improve our understanding of the spatial and temporal dynamics of both deforestation and forest degradation processes.

For the same time period assessed in this study, the PRODES deforestation mapping system reported a deforested area of 165,310 km^2 in the Brazilian Amazon [42], 2% less than our estimate (169,074 km^2). Differences between the total deforestation detected by the two monitoring systems are relatively small, but the intra-annual differences are high and have grown over time, with an absolute average difference of 2,270 km^2/year (Figure 7a). Differences between estimates from the two monitoring systems may result in part from any or all of the following factors: scale of monitoring, which is more detailed in the system we present (30m *vs*. 60m); misclassification of forest degradation

as deforestation; and estimation differences caused by the different dates of the annual images selected and varied annualization methods used to derive the annual deforestation rates from the satellite-based observations. Regardless, deforestation estimated by both monitoring systems presented similar patterns of high deforestation rates from 2001 to 2005, followed by a notable drop from 2006 to 2010. Our method has the added benefit of quantitatively mapping degraded forests in addition to annual deforestation integrated in the same method.

Forest degradation affected an area equivalent to 30% of the total area deforested during the period analyzed, with an average of 5,536 km^2 affected per year. Both selective logging and forest fires can impoverish forests in terms of biodiversity and carbon stocks [8,19,43], and thus it is critically important that these events are monitored annually to enable the effective establishment of Reduced Emissions from Deforestation and Forest Degradation ($REDD^+$) programs [44].

The method we present here for using Landsat satellite images to calculate annual rates of deforestation and forest degradation could become a much needed monitoring tool, both at the basin-scale and locally, to evaluate the performance of protected areas [45] and land management policies in controlling deforestation and resisting forest degradation. While our results show the encouraging trend of reduced deforestation rates in the Brazilian Amazon, they also illustrate the growing importance of forest degradation in recent years, averaging 49% of corresponding deforestation rates since 2006, *vs.* 21% in previous years. Annual forest degradation rates have increased by an average of 20% in recent years, even as deforestation rates have dropped. This same basin-wide trend has been seen in the increasing percentage of regional carbon loss attributable to forest degradation along edges of fragmented forests (growing at >3,000 km^2/yr 2006–2010), as landscape patterns have become more stable in recent years [11].

6. Conclusions

The combined area of forest that is being degraded by selective logging and forest fires each year may now equal or exceed the area being deforested, resulting in ever more fragmented landscapes. Basin-wide accounting of these processes is a necessary compliment to deforestation monitoring efforts if effective land management is to be practiced in this region. Our method only detects forest disturbances that results in >25% canopy opening. Therefore, very low intensity forest degradation created by non-mechanized logging, charcoal harvesting and other activities could not be effectively monitored using our methodology with Landsat imagery. More detailed spatial resolution imagery has the potential to detect and map these types of low intensity forest disturbances. The results from this research can now be used to investigate and quantify the possible interactions and transitions between classes of forest, forest degradation and deforestation, as well as the recurrence rates of disturbance events, providing for more effective modeling of how the ecological impacts and carbon emissions vary as a function of protected area status or associated land uses within this vital biome. With the new data becoming available from the recently launched Landsat 8 (LDCM: Landsat Data Continuity Mission), we intend to use this approach as the base for establishing an operational forest monitoring program in Brazil that can provide greater understanding of regional land cover dynamics and more precise estimates of historic carbon emission rates.

Acknowledgments

We would like to thank the Fundo Vale for support in developing the methodology for monitoring with Landsat images, image process activities and publication of this map. The ImgTools software had developmental support from the Moore Foundation, Climate Land Use Alliance and Fundo Vale. The Gordon & Betty Moore Foundation supported the satellite image processing team in monitoring forest degradation and deforestation in protected areas of the Amazon. The research also received support from NASA through the Biological Diversity Program to Dr. Mark Cochrane of South Dakota State University (Contract: NNX07AF16G) for operation activities in pre-processing and classifying images and the Terrestrial Ecology Program (NNX11AB89G) which has supported the involvement of Drs. Numata, Barber and Cochrane. The UK National Environment Research Council (NE/G000816/1), Instituto Nacional de Ciência e Tecnologia—Biodiversidade e Uso da Terra na Amazônia (CNPq 574008/2008-0) and NASA (NNX07AF16G) supported implementation of forest transects.

Conflict of Interest

The authors declare no conflict of interest in conducting this study.

References

1. Rosa, I.M.D.; Souza, C.; Ewers, R.M. Changes in size of deforested patches in the Brazilian Amazon. *Conserv. Biol.* **2012**, *26*, 932–937.
2. Shimabukuro, Y.E.; dos Santos, J.R.; Formaggio, A.R.; Duarte, V.; Rudorff, B.F.T. The Brazilian Amazon Monitoring Program. In *Global Forest Monitoring from Earth Observation*; Achard, F., Hansen, M.C., Eds.; CRC Press: Boca Raton, FL, USA, 2012; pp. 167–184.
3. Souza, C., Jr. Monitoring of Forest Degradation. In *Global Forest Monitoring from Earth Observation*; Achard, F., Hansen, M.C., Eds.; CRC Press: Boca Raton, FL, USA, 2012; pp. 185–208.
4. Numata, I.; Cochrane, M.A.; Roberts, D.A.; Soares, J.V.; Souza, C.M.; Sales, M.H. Biomass collapse and carbon emissions from forest fragmentation in the Brazilian Amazon. *J. Geophys. Res.: Biogeosci.* **2010**, *115*, G03027.
5. Nepstad, D.C.; Varissimo, A.; Alencar, A.; Nobre, C.; Lima, E.; Lefebvre, P.; Schlesinger, P.; Potter, C.; Moutinho, P.; Mendoza, E.; Cochrane, M.; Brooks, V. Large-scale impoverishment of Amazonian forests by logging and fire. *Nature* **1999**, *398*, 505–508.
6. Asner, G.P.; Knapp, D.E.; Broadbent, E.N.; Oliveira, P.J.C.; Keller, M.; Silva, J.N. Selective logging in the Brazilian Amazon. *Science* **2005**, *310*, 480–482.
7. Chen, Y.; Randerson, J T.; Morton, D.C.; DeFries, R.S.; Collatz, G.J.; Kasibhatla, P.S.; Giglio, L.; Jin, Y.; Marlier, M.E. Forecasting fire season severity in South America using sea surface temperature anomalies. *Science* **2011**, *334*, 787–791.
8. Skole, D.; Tucker, C. Tropical deforestation and habitat fragmentation in the Amazon—Satellite data from 1978 to 1988. *Science* **1993**, *260*, 1905–1910.

9. Asner, G.P.; Broadbent, E.N.; Oliveira, P.J.C.; Keller, M.; Knapp, D.E.; Silva, J.N.M. Condition and fate of logged forests in the Brazilian Amazon. *Proc. Natl. Acad. Sci. USA* **2006**, *103*, 12947–12950.
10. Matricardi, E.; Skole, D.; Cochrane, M.A.; Pedlowski, M.; Chomentowski, W. Multi-temporal assessment of selective logging in the Brazilian Amazon using Landsat data. *Int. J. Remote Sens.* **2007**, *28*, 63–82.
11. Numata, I.; Mark, A.C.; Carlos, M.S., Jr.; Marcio, H.S. Carbon emissions from deforestation and forest fragmentation in the Brazilian Amazon. *Environ. Res. Lett*. **2011**, *6*, 044003.
12. Cochrane, M.A.; Laurance, W.F. Fire as a large-scale edge effect in Amazonian forests. *J. Trop. Ecol.* **2002**, *18*, 311–325.
13. Souza, C.M., Jr.; Roberts, D.A.; Cochrane, M.A. Combining spectral and spatial information to map canopy damage from selective logging and forest fires. *Remote Sens. Environ.* **2005**, *98*, 329–343.
14. Alencar, A.; Asner, G.P.; Knapp, D.; Zarin, D. Temporal variability of forest fires in eastern Amazonia. *Ecol. Appl.* **2011**, *21*, 2397–2412.
15. Morton, D.C.; DeFries, R.S.; Nagol, J.; Souza, C.M., Jr.; Kasischke, E.S.; Hurtt, G.C.; Dubayah, R. Mapping canopy damage from understory fires in Amazon forests using annual time series of Landsat and MODIS data. *Remote Sens. Environ.* **2011**, *115*, 1706–1720.
16. Roberts, D.A.; Numata, I.; Holmes, K.; Batista, G.; Krug, T.; Monteiro, A.; Powell, B.; Chadwick, O.A. Large area mapping of land-cover change in Rondonia using multitemporal spectral mixture analysis and decision tree classifiers. *J. Geophys. Res.: Atmos.* **2002**, *107*, 8073.
17. Cochrane, M.A.; Souza, C.M., Jr. Linear mixture model classification of burned forests in the Eastern Amazon. *Int. J. Remote Sens.* **1998**, *19*, 3433–3440.
18. Laurance, W.F.; Camargo, J.L.C.; Luizao, R.C.C.; Laurance, S.G.; Pimm, S.L.; Bruna, E.M.; Stouffer, P.C.; Williamson, G.B.; Benitez-Malvido, J.; Vasconcelos, H.L.; Van Houtan, K.S.; Zartman, C.E.; Boyle, S.A.; Didham, R.K.; Andrade, A.; Lovejoy, T.E. The fate of Amazonian forest fragments: A 32-year investigation. *Biol. Conserv.* **2011**, *144*, 56–67.
19. Johns, J.S.; Barreto, P.; Uhl, C. Logging damage during planned and unplanned logging operations in the eastern Amazon. *Forest Ecol. Manage.* **1996**, *89*, 59–77.
20. Nepstad, D.C.; Verissimo, A.; Alencar, A.; Nobre, C.; Lima, E.; Lefebvre, P.; Schlesinger, P.; Potter, C.; Moutinho, P.; Mendoza, E.; Cochrane, M.; Brooks, V. Large-scale impoverishment of Amazonian forests by logging and fire. *Nature* **1999**, *398*, 505–508.
21. Souza, C.M.; Roberts, D.A.; Cochrane, M.A. Combining spectral and spatial information to map canopy damage from selective logging and forest fires. *Remote Sens. Environ.* **2005**, *98*, 329–343.
22. Souza, C., Jr.; Siqueira, J.V. ImgTools: A Software for Optical Remotely Sensed Data Analysis. In Proceeding of Anais XVI Simpósio Brasileiro de Sensoriamento Remoto, Foz do Iguaçu, PR, Brazil, 13–18 April 2013; pp. 1571–1578.
23. Verbyla, D.L.; Boles, S.H. Bias in land cover change estimates due to misregistration. *Int. J. Remote Sens.* **2000**, *21*, 3553–3560.
24. Carlotto, M.J. Reducing the effects of space-varying, wavelength-dependent scattering in multispectral imagery. *Int. J. Remote Sens.* **1999**, *20*, 3333–3344.

25. Roberts, D.A.; Adams, J.B.; Sabol, D.E. Remote sensing of vegetation in Amazonia, ecological implications of spectral mixtures. *Bull. Ecol. Soc. Amer.* **1993**, *74*, 412.
26. Adams, J.B.; Sabol, D.E.; Kapos, V.; Filho, R.A.; Roberts, D.A.; Smith, M.O.; Gillespie, A.R. Classification of multispectral images based on fractions of endmembers: Application to land-cover change in the Brazilian Amazon. *Remote Sens. Environ.* **1995**, *52*, 137–154.
27. Roberts, D.A.; Numata, I.; Holmes, K.; Batista, G.; Krug, T.; Monteiro, A.; Powell, B.; Chadwick, O.A. Large area mapping of land-cover change in Rondônia using multitemporal spectral mixture analysis and decision tree classifiers. *J. Geophys. Res.: Atmos.* **2002**, *107*, 8073.
28. Asner, G.P.; Bustamante, M.M.C.; Townsend, A.R. Scale dependence of biophysical structure in deforested areas bordering the Tapajo's National Forest, Central Amazon. *Remote Sens. Environ.* **2003**, *87*, 507–520.
29. Numata, I.; Soares, J.V.; Roberts, D.A.; Leonidas, F.C.; Chadwick, O.A.; Batista, G.T. Relationships among soil fertility dynamics and remotely sensed measures across pasture chronosequences in Rondonia, Brazil. *Remote Sens. Environ.* **2003**, *87*, 446–455.
30. Souza, C.M., Jr.; Firestone, L.; Silva, L.M.; Roberts, D. Mapping forest degradation in the Eastern Amazon from SPOT 4 through spectral mixture models. *Remote Sens. Environ.* **2003**, *87*, 494–506.
31. Small, C. The Landsat ETM+ spectral mixing space. *Remote Sens. Environ.* **2004**, *93*, 1–17.
32. Asner, G.P.; Keller, M.; Pereira, R.; Zweede, J.C. Remote sensing of selective logging in Amazonia—Assessing limitations based on detailed field observations, Landsat ETM+, and textural analysis. *Remote Sens. Environ.* **2002**, *80*, 483–496.
33. Boardman, J.W.; Kruse, F.A.; Green, R.O. Mapping Target Signatures via Partial Unmixing of AVIRIS Data. In Proceedings of Annual JPL Airborne Geoscience Workshop, Pasadena, CA, USA, 23–26 January 1995; pp. 23–26.
34. Powell, R.L.; Matzke, N.; de Souza, C.; Clark, M.; Numata, I.; Hess, L.L.; Roberts, D.A.; Clark, M.; Numata, I.; Hess, L.L.; Roberts, D.A. Sources of error in accuracy assessment of thematic land-cover maps in the Brazilian Amazon. *Remote Sens. Environ.* **2004**, *90*, 221–234.
35. Souza, C.M., Jr.; Cochrane, M.A.; Sales, M.H.; Monteiro, A.L.; Millicone, D. *Integrating Forest Transects and Remote Sensing Data to Quantify Carbon Loss due to Forest Degradatin in the Brazilian Amazon*; Forest Resource Assessment Working Paper 161; FAO: Rome, Italy, 2009; pp. 1–17.
36. Asner, G.P. Cloud cover in Landsat observations of the Brazilian Amazon. *Int. J. Remote Sens.* **2001**, *22*, 3855–3862.
37. FAO. On Definitions of Forest and Forest Change. In *Food and Agriculture Administration, Forest Resource Assessment*; Working Paper 33; FAO: Rome, Italy, 2000; p. 13.
38. Puyravaud, J.P. Standardizing the calculation of the annual rate of deforestation. *Forest Ecol. Manage.* **2003**, *177*, 593–596.
39. Cochrane, M.A.; Alencar, A.; Schulze, M.D.; Souza, C.M.; Nepstad, D.C.; Lefebvre, P.; Davidson, E.A. Positive feedbacks in the fire dynamic of closed canopy tropical forests. *Science* **1999**, *284*, 1832–1835.
40. Davidson, E.A.; de Araujo, A.C.; Artaxo, P.; Balch, J.K.; Brown, I.F.; C. Bustamante, M.M.; Coe, M.T.; DeFries, R.S.; Keller, M.; Longo, M.; *et al*. The Amazon basin in transition. *Nature* **2012**, *481*, 321–328.

41. Soares-Filho, B.S.; Nepstad, D.C.; Curran, L.M.; Cerqueira, G.C.; Garcia, R.A.; Ramos, C.A.; Voll, E.; McDonald, A.; Lefebvre, P.; Schlesinger, P. Modelling conservation in the Amazon basin. *Nature* **2006**, *440*, 520–523.
42. INPE. Prodes, Monitoramento da Floresta Amazônica por Satélite. Available online: http://www.obt.inpe.br/prodes/index.php (accessed on 6 May 2013).
43. Barlow, J.; Peres, C.A.; Henriques, L.M.P.; Stouffer, P.C.; Wunderle, J.M. The responses of understorey birds to forest fragmentation, logging and wildfires: An Amazonian synthesis. *Biol. Conserv.* **2006**, *128*, 182–192.
44. Barlow, J.; Parry, L.; Gardner, T.A.; Ferreira, J.; Aragao, L.E.O.C.; Carmenta, R.; Berenguer, E.; Vieira, I.C.G.; Souza, C.; Cochrane, M.A. The critical importance of considering fire in REDD+ programs. *Biol. Conserv.* **2012**, *154*, 1–8.
45. Barber, C.P.; Cochrane, M.A.; Souza, C.; Verissimo, A. Dynamic performance assessment of protected areas. *Biol. Conserv.* **2012**, *149*, 6–14.

© 2013 by the authors; licensee MDPI, Basel, Switzerland. This article is an open access article distributed under the terms and conditions of the Creative Commons Attribution license (http://creativecommons.org/licenses/by/3.0/).